Inter J Nav Archit Oc Engng (2012) 4:44~56
http://dx.doi.org/10.2478/IJNAOE-2013-0077

Shape optimization of an autonomous underwater vehicle with a ducted propeller using computational fluid dynamics analysis

Tae-Hwan Joung[1], Karl Sammut[1], Fangpo He[1] and Seung-Keon Lee[2]

[1]*School of Computer Science, Engineering and Mathematics, Flinders University, Adelaide, Australia*
[2]*Department of Naval Architecture and Ocean Engineering, Pusan National University, Bu-san, Korea*

ABSTRACT: *Autonomous Underwater Vehicles (AUVs) provide a useful means of collecting detailed oceano-graphic information. The hull resistance of an AUV is an important factor in determining the power requirements and range of the vehicle. This paper describes a procedure using Computational Fluid Dynamics (CFD) for determining the hull resistance of an AUV under development, for a given propeller rotation speed and within a given range of AUV velocities. The CFD analysis results reveal the distribution of the hydrodynamic values (velocity, pressure, etc.) around the AUV hull and its ducted propeller. The paper then proceeds to present a methodology for optimizing the AUV profile in order to reduce the total resistance. This paper demonstrates that shape optimization of conceptual designs is possible using the commercial CFD package contained in Ansys™. The optimum design to minimize the drag force of the AUV was identified for a given object function and a set of constrained design parameters.*

KEY WORDS: AUV (Autonomous Underwater Vehicle); CFD (Computational Fluid Dynamics); Design optimization; Drag force; Drag coefficient (C_D); Sensitivity.

INTRODUCTION

An Autonomous Underwater Vehicle (AUV) is a versatile research tool for defence applications, oil, gas and mineral exploration programs, and for maritime archaeology, oceanographic and marine biology studies. Rapid progress in AUV development is steadily increasing the reliability and endurance of such vehicles to operate in harsh marine environments. Much work, however, still needs to be done in terms of automating the process of optimizing hull designs to minimize drag and increase propulsion efficiency.

In previous studies reported in the literature, designers have employed empirical formulae or used experimental derived data to estimate drag force of ships or submerged body such as AUVs (Barros, 2006). However, conventional empirical formulas are not able to accurately compute the drag of complex hull forms with appendages protruding from the hull. Although experimental testing using a tow tank and or cavitation tank can produce very accurate predictions of drag, such testing requires considerable time and effort, and expensive test facilities to obtain the hydrodynamic characteristics of the vehicle. Consequently, a new drag estimation method, which is more cost-efficient, reliable and also convenient for designers, is needed for development of a new conceptual design of AUVs.

In this paper, Computational Fluid Dynamics (CFD) tools are evaluated with the purpose of estimating the hydrodynamic parameter characteristics (drag, velocity, pressure etc.) of an AUV with a ducted propeller. The design of a concept torpedo-shaped AUV is optimized using CFD analysis to minimize drag force.

The methods reported in this paper for optimization by CFD code are as follows: (1) CFD analysis and validation by comparison with theoretical equation and empirical testing, (2) an automatic element meshing method that generates a boun-

Corresponding author: *Tae-Hwan Joung, Karl Sammut*
e-mail: *joun0001, karl.sammut@flinders.edu.au*

dary layer which allows for appendages such as fins and ducts, and produces a stable and robust analysis, and (3) searching and identifying optimum values of design variables (such as the nozzle angle) to produce minimum resistance.

INITIAL HULL DESIGN AND DRAG ESTIMATION OF THE AUV

Hull design

At a conceptual design stage, the hull of an AUV can be divided into four distinct sections, namely the *nose*, *middle*, *tail* and *propulsion* (propeller and duct) sections. The hull has been designed based on the Myring hull profile equations (Myring, 1976) which are known to produce minimum drag force for a given fineness ratio (*l*/*d*), that is, the ratio of its length to its maximum diameter. The shapes of the nose and tail sections are determined from (1) and (2), respectively:

$$r(x) = \frac{1}{2} d \left[1 - \left(\frac{x-a}{a} \right)^2 \right]^{1/n} \tag{1}$$

$$r(x) = \frac{1}{2} d - \left[\frac{3d}{2c^2} - \frac{\tan(\theta)}{c} \right] (x-(a+b))^2 + \left[\frac{d}{c^3} - \frac{\tan(\theta)}{c^2} \right] (x-(a+b))^3 \tag{2}$$

where, *r(x)* is the radius at a point along the *x*-axis, *a*, *b* and *c* are the lengths of the nose, body and tail sections, respectively, *d* is the maximum diameter, *n* is an exponential parameter which can be varied to give different body shapes, and θ is the included angle at the tip of the tail.

The concept design of the AUV hull with its ducted propeller is shown in Fig. 1. As each propeller blades rotates through the water, they generate high pressure areas behind the blade and low pressure areas ahead of the blade. It is this pressure differential that provides the force to drive the vessel. In the case of an unducted propeller, however, losses occur at the blade tips as water escapes from the high pressure side of the blade to the low pressure side, resulting in reduced efficiency in terms of pushing the vessel forward. To obtain the most thrust, a propeller must move as much water as possible in a given time. A duct or nozzle will reduce these propeller losses, especially when a high thrust is needed at a low vehicle speed (Barringhaus and Olds, 2007). A *Rice* nozzle with a NACA 6721 profile has been employed for our AUV design concept, since its coefficient of drag is over 17 times less than that of a conventional *Kort* nozzle. The characteristics of the designed nozzle are given in Table 1.

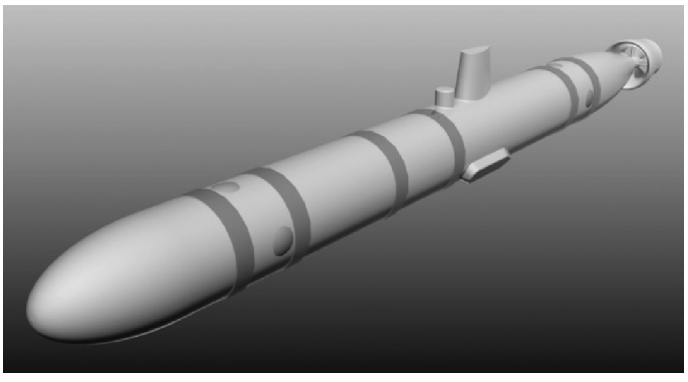

Fig. 1 A conceptual design of the flinders AUV.

Table 1 Nozzle profile - (NACA 6721) .

Thickness	21	% of wing chord (Length of chord = 1)
Position	0.7	Position of maximum camber (0 - 1)
Camber	0.06	% of wing chord (Length of chord = 1)

Estimation of the resistance factor by an empirical formula

The drag caused by an axis-symmetric AUV moving forward through the water is a direct result of the viscosity of the water. The effect of viscosity can be considered as two separate factors. That is, one is the skin friction drag which is caused by the viscosity shear force of a fluid flowing along the hull, and the other is the form drag caused by development of a boundary layer and the resulting difference of pressure distribution between front and stern of the vehicle (Phillips, et al., 2007). To estimate the coefficient of friction drag (C_F) caused by viscosity, the *ITTC 1957 correlation line* (Edward, 1988), which is a commonly used method for estimation of the skin friction component, is considered here.

The correlation line as a function of Reynolds number, R_N, can be considered as follows:

$$C_{F_{1957}} = \left(\frac{0.075}{\log(R_N - 2)^2} \right) \tag{3}$$

The coefficient of the friction drag (C_F), however, should be multiplied by the form factor (1+k), which is a function of the hull shape, in order to complete the estimation. Hoerner (Hoerner, 1965) proposed the form factor as a function of the hull length (l) and hull diameter (d) as follows:

$$(1+k) = 1 + 1.5(d/l)^{3/2} + 7(d/l)^3 \tag{4}$$

Estimation of the drag force

The axial drag force acting on a body moving at a constant velocity in a fluid medium is approximated by (5). The drag force of an AUV, therefore, can be estimated by using the following formula (Michael, 2003).

$$R_f = \frac{1}{2}\rho C_f A_f |u|u = X_{|u|u}|u|u \tag{5}$$

where, C_f is the coefficient of friction drag obtained from equation (3) and (4), ρ is the density of the fluid, A_f is the submerged surface area of the hull, and u is the fluid velocity or the advance speed of the AUV. This estimation for the drag force can provide useful information for the propulsion requirements at the early stages of a design. However, the estimation of the drag coefficient obtained only by considering form factor (1+k) can be uncertain, particularly when complex shaped equipment such as, antennas, acoustic communications transducers, side scan sonar transducers, or other protruding equipment, are attached to the AUV hull.

AUV DRAG ESTIMATION USING CFD ANAYSIS

Governing equation of the CFD analysis

The fluid flow around the AUV has been modelled using the commercial CFD code ANSYS CFX 13.0. For these calculations, the governing equations are the Navier-Stokes equations and the continuity equation under the assumption of incompressible fluid. The Navier-Stokes equations employed in CFX is the isothermal Reynolds Averaged Navier-Stokes (RANS) (Wilcox, 1998), as given in (7).

$$\frac{\partial v_j}{\partial x_j} = 0 \tag{6}$$

$$\frac{\partial \rho v_i}{\partial t} + u_i \frac{\partial \rho v_i}{\partial x_j} = -\frac{\partial p}{\partial x_i} + \frac{\partial \tau_{ij}}{\partial x_i} + F_i \tag{7}$$

where Einstein's summation convention is adopted, i.e., x_j (j=1,2,3) denotes the axes of the orthogonal coordinate system (see Fig. 2). The x_3 axis is parallel with the longitudinal (x) axis of the fuselage, pointing from nose to tail. t is time; v_i is the i-th component of the fluid velocity; ρ is a density of the fluid; τ_{ij} is a viscosity stress tensor; and F_i is the external force (body force) of i-th element due to the gravity, thrust power and torque.

Pre-processing for CFD analysis

Modelling for CFD analysis

The Myring and NACA equations for the hull and nozzle geometries, respectively, were computed in MS-EXCEL and exported to *ANSYS Workbench Design Modeller*. The 3D model was then meshed using *ANSYS-CFX-MESH*. ANSYS-CFX-MESH was also employed for the optimization process, because of its auto-meshing function and its link-up with *ANSYS-Design Exploration*, which is the optimization program in ANSYS-Workbench.

Mesh generation (Hybrid mesh)

'Tetrahedral' and 'Pyramid' meshes are normally employed for generating nodes and elements in the fluid domain. While 'Tetrahedral' and 'Pyramid' meshes are suitable for representation of a complex geometry such as a nozzle, they are not suitable to resolve the boundary layers adjacent to a solid body (Nishi, 2007). Instead, 'Prism' meshes, which are the most appropriate element for this purpose (ANSYS, 2009), are used for generating the boundary layer elements around the body.

Fig. 3 (a), (b) and (c) show the various meshed sections which are merged for the CFD analysis by the mesh generator. The size of the fluid domain around the tank is big enough so as to not cause any error due to blocking effects which can occur when the size of the tank is so small that the walls of the tank significantly restrict flow around the hull.

The shape of the domain is cylindrical as shown in Fig. 3 (a). The length of the domain is 2.5L and diameter is 10D. The length of the tank behind of the AUV (1.67L) is longer than the length of the tank (0.83L) forward of the AUV so as to allow the wake from the AUV body to be observed.

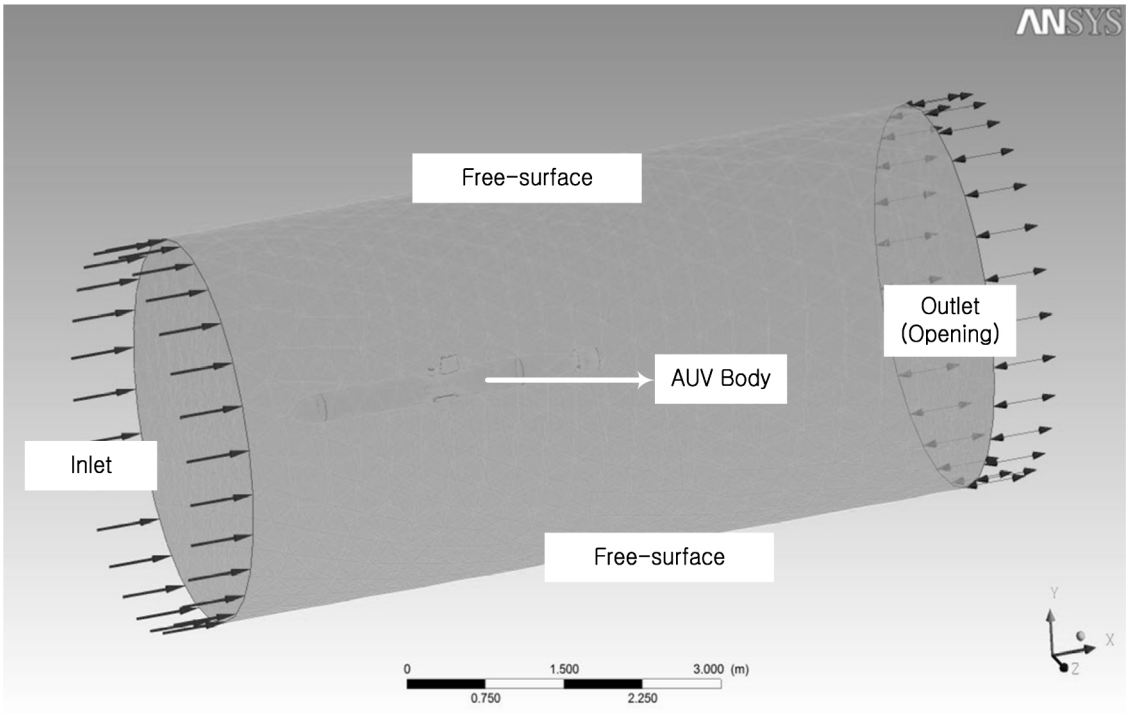

Fig. 2 Overview of the pre-processing for the CFD analysis.

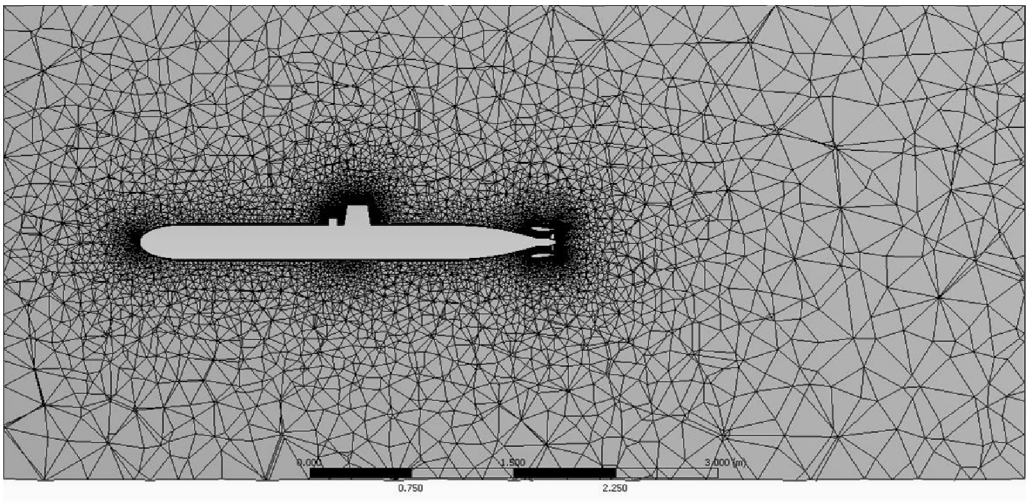

(a) Side view (Total).

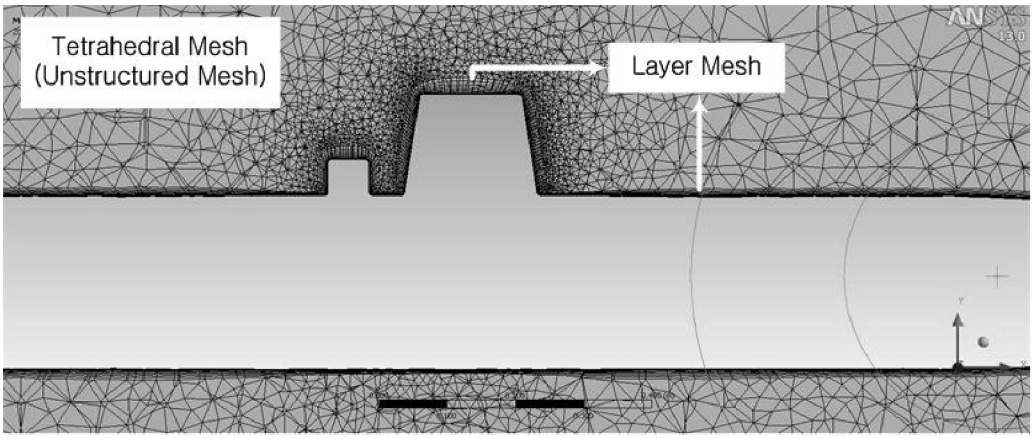

(b) Side view (Mid-section).

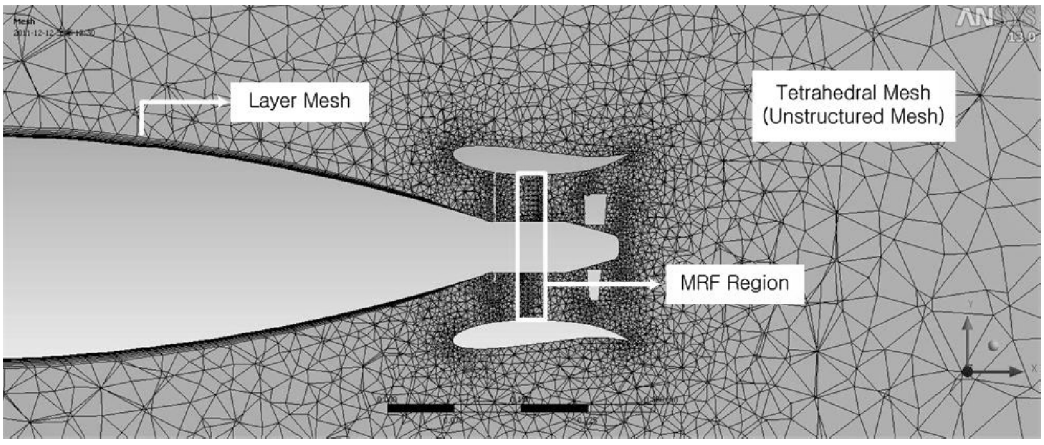

(c) Side view (Propulsion section).

Fig. 3 Hybrid (Tetrahedral and Layer) meshes generated adjacent to the main body and nozzle of the AUV.

In order to determine the velocity of the AUV, the inlet velocity at the front of the water tank was set to be equivalent to the advance AUV velocity while the constraint given to the outlet (opposite side of the inlet) was set to the *opening* option which has no relative pressure. The *Free Surface Condition* was allocated to the remaining cylindrical surface of the water tank as shown in Fig. 2.

Turbulence model

Various turbulence models, such as *k-epsilon* (k-ε), *Shear Stress Transport* (SST), *BSL Reynolds Stress*, and *SSG Reynolds Stress* models, are capable of providing solutions to the Reynolds stresses in terms of known quantities to allow closure of the RANS equations by ANSYS CFX (Wilcox, 1998).

The k-ε model and the SST were shortlisted out of the possible set of turbulence models as possible candidates for this study. The reason for this selection is that the k-ε model is a commonly used turbulence model for engineering simulations due to its robustness and applicability to a wide range of flows, while the SST model is better at predicting separation (ANSYS, 2009) likely to be found aft of the AUV. From CFD analysis of the AUV, the drag predictions from SST and k-ε model have a high degree of correspondence.

The k-ε turbulent model was, however, ultimately chosen for the optimization stage, due to its compatibility with the mesh generation tools and its capacity to generate less numbers of elements when auto meshing. The scalable wall function was employed near the AUV body wall to enhance accuracy and reduce computation time. The height of cells adjacent to the walls was set to less than 100 y+ units for compatibility with the k-ε turbulent model at low Reynolds numbers (ANSYS, 2009) and the wall function. y+ is a non-dimensional description of distance from a wall in relation to local flow and wall shear stress parameters as shown in (8). The expression of distances from the wall in y+ 'units' is important in defining velocity and turbulence distributions in a universal form suited to wall functions.

$$y+ = \frac{yU_\tau}{\nu} \tag{8}$$

where U_τ is the friction velocity (τ_w/ρ) and ν is kinematic viscosity coefficient.

Moving Reference Frame (MRF)

There are several existing CFD methods for representing propeller characteristics. The *Moving Reference Frame* (MRF) and the *Sliding Mesh Method* (SMM) are two typical methods. The SMM offers the most accurate numerical representation of a propeller behaviour but is very time consuming and computationally demanding which makes it impractical for complex applications. The MRF model is a steady state approximation where the fluid zone encompassing the propeller region, as shown by the box around the propeller in Fig. 2 (c), is modelled in a rotating frame of reference while the surrounding zones are modelled in a stationary frame. Frozen propeller interfaces are used to connect the rotating and stationary domains. For the purposes of the shape optimization process, the rotational speed of the propeller was set to 800 rpm with the MRF method. The specifications for the *pre-processing* stage, including the mesh generation, are summarized in Table 2.

CFD ANAYSIS AND RESULTS

Procedure for the CFD analysis

The CFD analysis module provided with ANSYS-CFX is easy to use and allows solutions to be quickly generated by control of the iteration times. In addition, the tool is also able to provide a satisfactory reliability analysis result with the desired degree of convergence.

The commercial code allows users the ability to supervise variations to the object function such as momentum, pressure, force, etc., while it is computing. If the results reach a predetermined value, a user can stop the run and move to the post-processing phase to evaluate the results. Fig. 5 shows the solve-process phase being monitored while ANSYS-CFX solver is running. Note that the value of the drag force along the X-axis of the AUV converged after nearly 40 iterations. The user can, therefore, decide on the number of iterations for convergence and determine when to stop in order to save CPU time.

Verification

In order to verify the results of the CFD analysis, the bare hull of the AUV, excluding the nozzle, propeller, sail and other projecting transducers, was analysed using the CFD tools and compared against the ITTC 1957 (Edward, 1988) benchmark.

The drag force predictions from the CFD results and the 'form factor (1+*k*) corrected ITTC 1957 correlation line' have a high degree of correspondence as shown in Fig. 4. The results show that the form factor predicted by (4) is useful for estimation purposes. There is, however, some difference in drag between the ANSYS-CFX computed values and the 'form factor corrected ITTC 1957 correlation line', because ANSYS-CFX considers the total drag while the ITTC 1957 correlation line considers only the skin friction drag. The CFD results can thus be regarded as valid and con-sidered to be reliable and useful for further research such as optimizing the nozzle shape.

Table 2 Principal conditions employed in the CFD analysis.

Water tank size	2.5*m* (ahead of AUV), 5.0*m* (behind AUV), 3.5*m* (Diameter)
Turbulence model	k-ε model (Scalable wall function)
Reynolds number	$1.54 \times 10^5 - 4.6 \times 10^6$
Y+ check	< 100
AUV dimensions	0.254*m* (Diameter), 3.060*m* (Length)
Total no. of elements (nodes)	797,494 (180,924)
No. of Tetrahedral elements	687,392
No. of Prism elements	109,783
RPM (Propeller)	800*rpm* (MRF)

The CFD results

The empirical results obtained from ITTC1957, however, do not include the effects of separation or vortices at the stern. The detailed information about the velocity and pressure distribution of the AUV with nozzle can be extracted from the CFD code, ANSYS-CFX.

The pressure distribution around the AUV, as shown in Fig. 6, reveals an even distribution except for the stagnation points at the bow and in the front of the transducer and the sail. The maximum pressure (1.227E3Pa) occurs at those stagnation points and the minimum pressure (-4.652E3Pa) occurs within part of nozzle. The negative pressure is higher in magnitude compared to the pressure along the main body of the AUV.

The coefficients of pressure and skin friction distribution along the AUV are shown in Fig. 7. Since the coefficient of skin friction (C_F) is so small compared to the coefficients of pressure (C_P), C_F is scaled up by 100 so that it can be seen in the same plot as C_P.

As the fluid passes along the cylindrical mid-body section towards the stern and then along the converging tail profile, the boundary layer grows and the flow accelerates as it reaches the nozzle as shown in Fig. 8. Large vertical structures which represent the wake region form behind the stern as shown in Fig. 8. The flow is accelerated around the nozzle up to a maximum velocity of $4.562U_0$, where U_0 is the inlet velocity. The maximum velocity of the fluid in the nozzle is thus 7.04m/s when the AUV velocity is 1.5432 m/s (3 knots) for a given propeller speed of 800rpm.

CFD ANAYSIS BASED OPTIMIZATION

Design optimization method

Having developed an initial concept design for the AUV profile, the next stage was to optimize the design in order to minimise drag…. Three design variables (DV1- DV3) are considered as shown in Fig. 9.

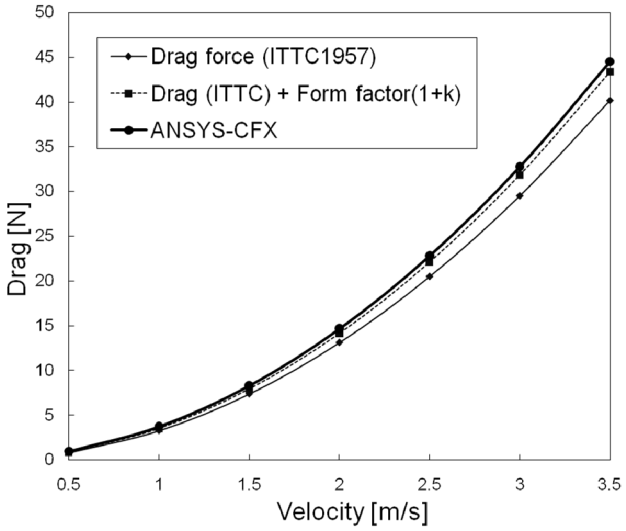

Fig. 4 Comparisons of drag predictions for the AUV body only (Bare hull only).

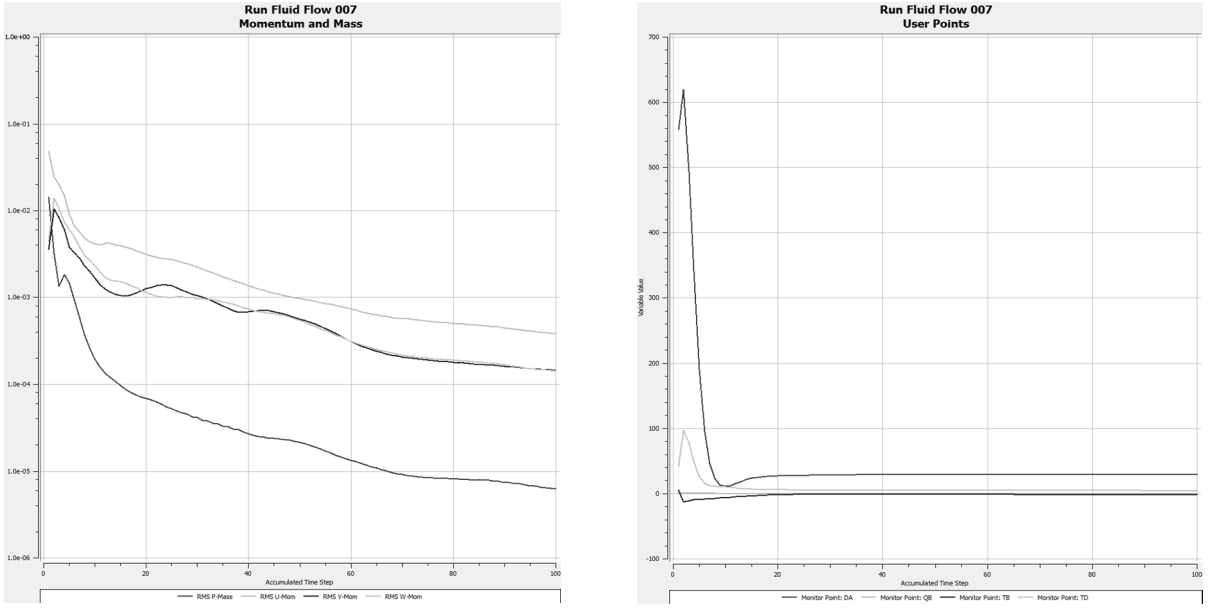

(a) Default (Momentum etc.). (b) Defined by user (Drag).

Fig. 5 Monitoring during the CFD analysis process at 3knots.

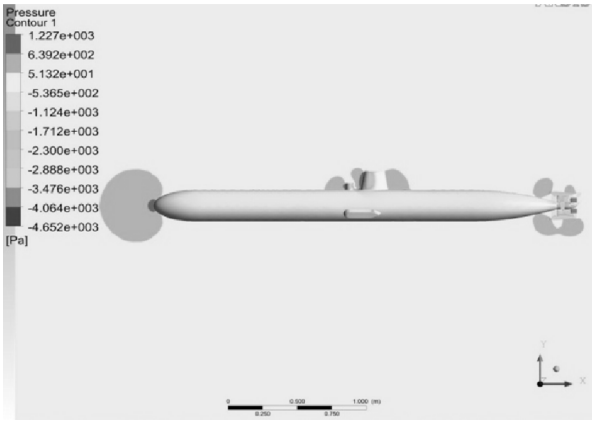

Fig. 6 Pressure contours around the AUV hull at 3knots.

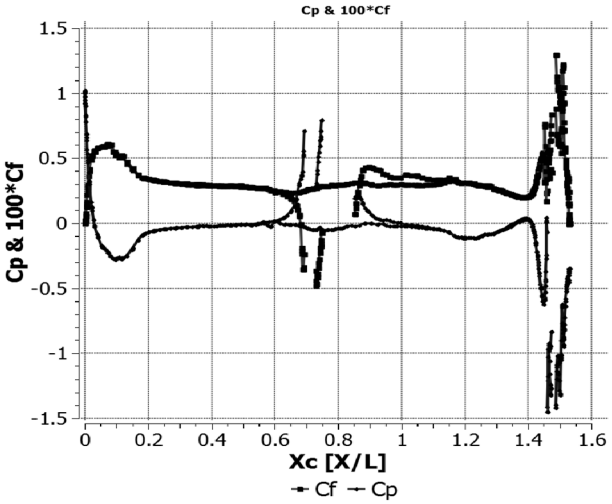

Fig. 7 C_p and $100\times C_f$ distribution around the AUV at 3knots.

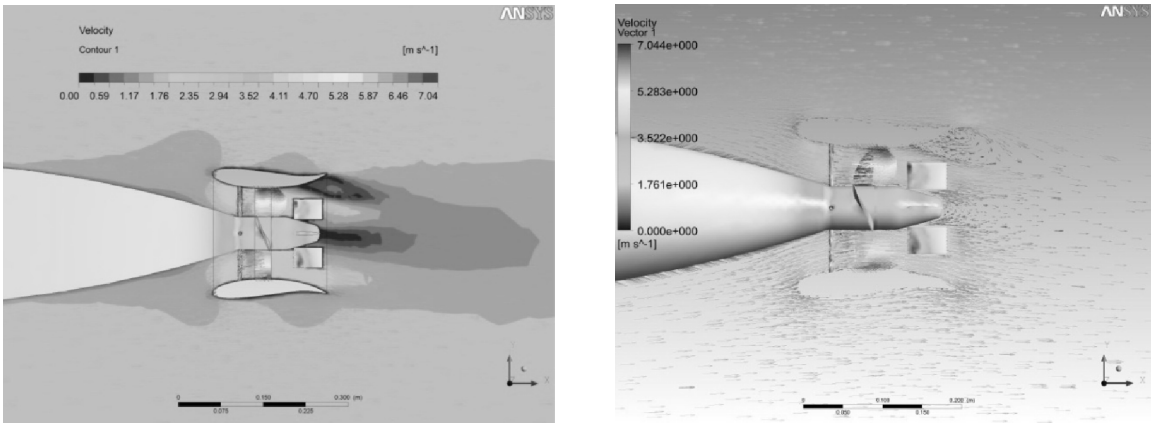

Fig. 8 Velocity contour and velocity profile at 3knots.

DV1 specifies the location of the sail relative to the bow,

DV2 specifies the separation between the sail and the acoustic communications transducer,

DV3 specifies the angle of attack of the nozzle (Ψ).

All of the design variables satisfy the given constraints, shown in Table 3, in order to minimize the overall drag resistance of the AUV body at a given speed (1-3knots) and RPM (800rpm) of the propeller. Given that this duct is most efficient at low speeds and less efficient at high speeds due to the added drag of the nozzle, the range of speeds analysed is 1- 3 knots.

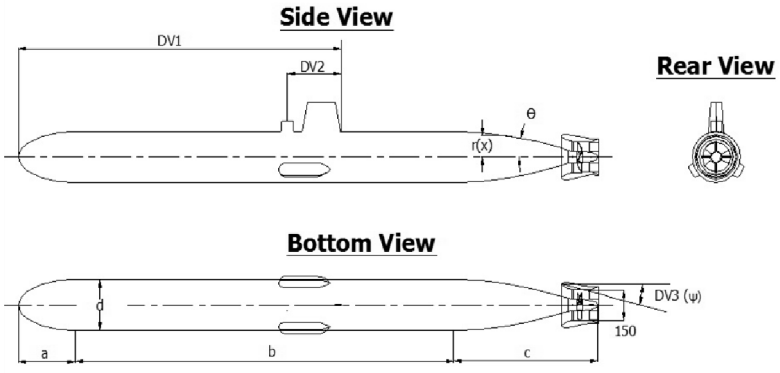

Fig. 9 A conceptual design of the AUV.

A design optimization procedure was therefore conducted to find the optimum value of the design variables (input parameters:- DV1, DV2 and DV3) considering given constraints (shown in Table 2) and the object function (output parameter:- drag force along X-axis).

Table 3 Design variables constraints.

DV1	Location of the sail	1400*mm* ≤ DV1≤ 2000*mm*
DV2	Separation between sail and transducer	240*mm* ≤ DV2≤ 320*mm*
DV3	Angle of attack of the nozzle	0° ≤ DV3(Ψ) ≤ 20°
Sail length		200*mm*
Communications Transducer Diameter		50*mm*

For the purpose of finding the optimum value of the object function, the three tools, that is, the 3D-CAD program, the mesh generation program and ANSYS-Design Exploration, must be linked together. ANSYS-Design Exploration is the optimization program, which sets up the relationships between the input parameter from the 3D CAD program (Design Modeler (DM), AUTOCAD etc.) and the output parameters.

ANSYS-Design Exploration offers two different workflows as shown in Fig. 10. External CAD software is used for 3D modelling in place of Design Modeler inside ANSYS-Workbench in Method 1. On the other hand, Design Modeler is used for 3D modelling in Method 2 as it is able to save computation time and is more easy to use. For the purposes of this study, Method 2 has been chosen for optimization of the three design variables.

The ANSYS-Design Exploration provides the *Design of Experiments* (DOE) method. Within the optimization process, DOE is used to create a matrix and build an approximation model. Optimization is then performed by sampling against this approximation model. The *Central Composite Design* (CCD) is a design widely used for estimating second order response surfaces. A *Box-Wilson Central Composite Design*, commonly called a *central composite design*, contains an embedded factorial or fractional factorial design with center points that is augmented with a group of *star points* that allow estimation of curvature. In this study, the sampling points are selected by the CCD method to carry out the DOE optimisation, before finding the optimum value of the design variable. That is, sample points are abstracted by CCD, and the optimal design variable which has the optimum value of the object function are then identified.

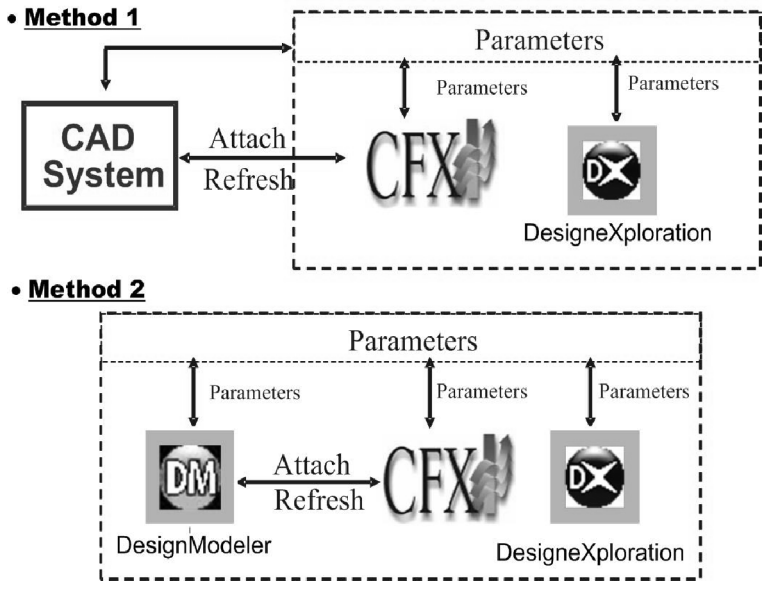

Fig. 10 Typical ANSYS-design exploration workflow.

Results of the design optimisation

The optimum values for the design variables for a range of speeds from 1 knot to 3 knots as identified from the DOE method, are shown in Table 4. From the results it can be seen that as the location of the sail moves aft, i.e., DV1 in-creases, the drag force is reduced. Conversely, as the distance between sail and transducer, i.e., DV2, increases, it plays a less significant role on the total drag force at higher speeds (i.e. 2 to 3 knots). This is due to the separation of flow past the transducer which is not as significant at lower speeds.

The relative sensitivities of the design variables are shown in Fig. 11 where DV3 can clearly be seen to be by far the most significant factor, compared to DV1 and DV2, in determining the total drag of the AUV throughout from 1 knot to 3 knots.

As shown in Table 4 and Fig. 12, the optimum value of DV3 (Ψ) is determined to be 8.19° at 1 knot and 9.15° at 2 knots and 3 knots; and the values of the object function (drag force) were -2.47 N at 1 knot, 8.59 N at 2 knots, and 20.21 N at 3 knots.

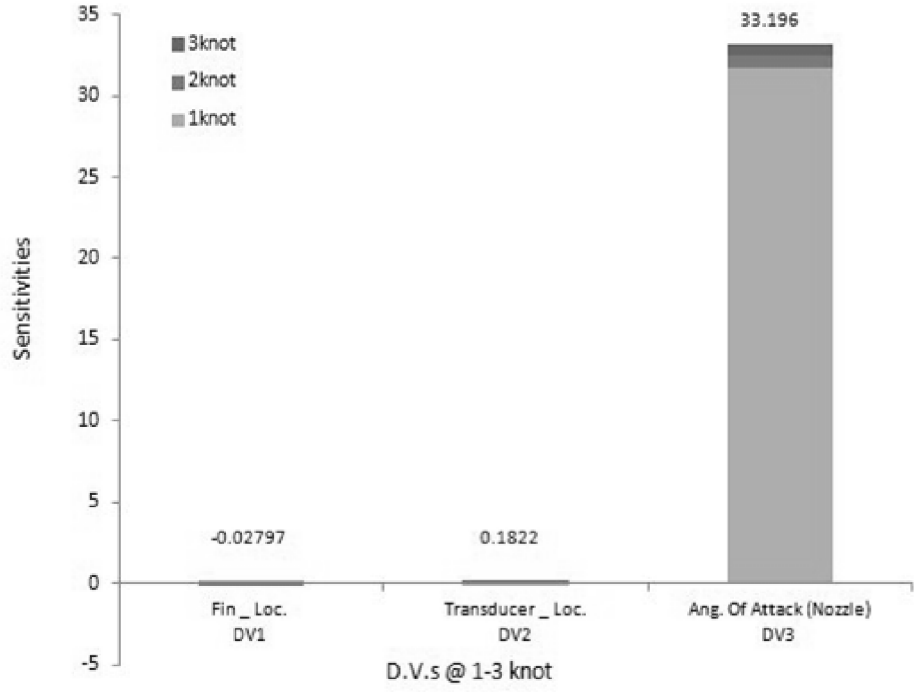

Fig. 11 Sensitivity of the drag force to changes in the design variables at the optimal design point of the AUV.

Table 4 Optimized values of the design variables.

Velocity	Input parameters			Object function
	DV1[*mm*]	DV2[*mm*]	DV3 [*deg.*]	Drag force [*N*]
Initial value	*1700.00*	*280.00*	*0*	-
1 knot	1990.34	240.68	8.19	-2.4744
2 knot	1981.55	317.48	9.15	8.5930
3 knot	1981.55	317.48	9.15	20.2128

From the results of the CFD analysis, shown in Fig. 12 and illustrated in Fig. 13(b), it can be seen that if the nozzle angle for a speed of 3 knots is less than the optimum angle i.e., 9.15°, then the value of the drag force increases relative to the drag force at the optimum angle. Conversely, as shown in Fig. 13(d), even though more mass flow of the water is admitted through the nozzle when the nozzle angle is greater than optimum angle, not only does the drag force become much higher, but also vortices can occur behind the nozzle which reduces the nozzle efficiency.

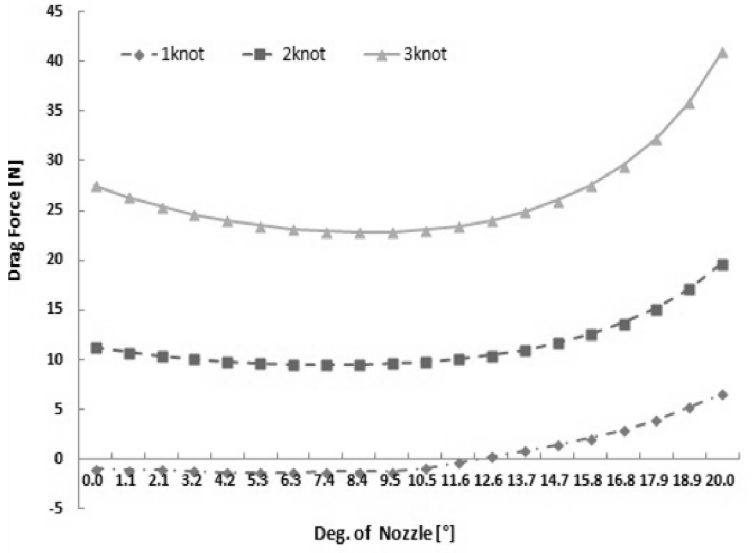

Fig. 12 X-directional drag force acting on the AUV (DOE).

The most significant observation is that when the angle of attack of the nozzle is less than 11° at low speed (1 knot), advance thrust is larger than the drag force so that the value of the total drag force is negative, i.e., the direction of the drag force is in the forward direction.

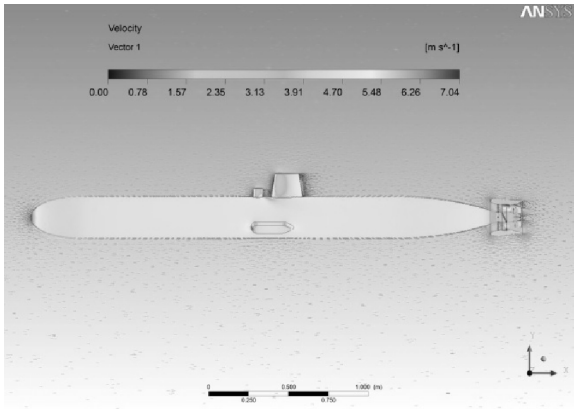

(a) Pressure and velocity contours.

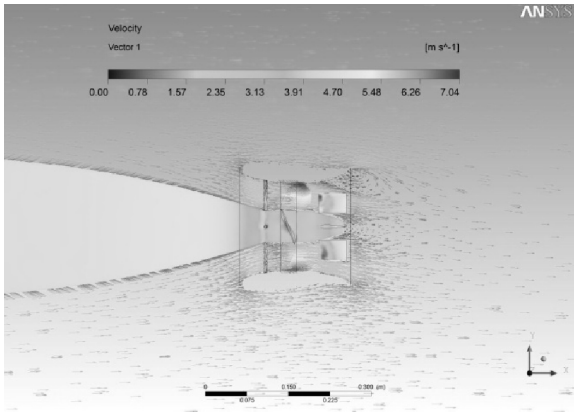

(b) 0° Nozzle angle (Initial value).

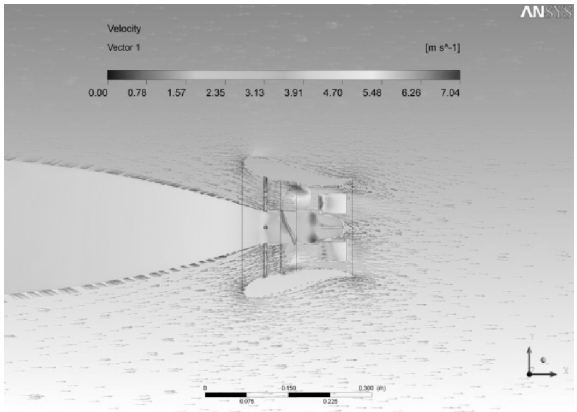

(c) 9.15 Nozzle angle (Optimum value).

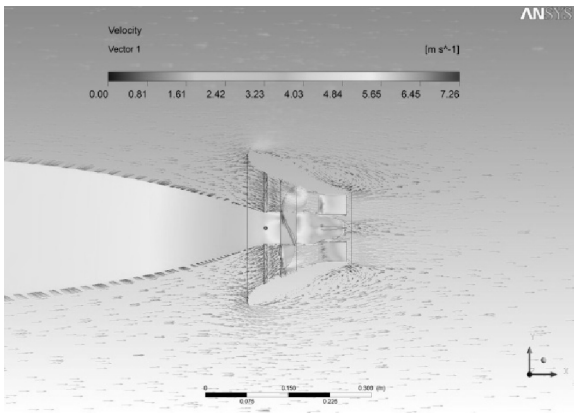

(d) 20° Nozzle angle.

Fig. 13 Pressure and velocity contours at 3 knots.

CONCLUSIONS

In this paper, an AUV concept design has been modelled, automatically meshed, and analysed using a commercial CFD program to assess the AUV's drag characteristics. As a result of the CFD analysis, pressure and velocity distribution measurements, and drag force measurements taken around the AUV were obtained.

The CFD analysis was then ex-tended to study the effectiveness of using the tools to optimize the design of the vehicle based on its drag behaviour by modifying the position of its sail and communications transducer, and by modifying the angle of attack of the propulsion nozzle. In summarizing the results of this study, we conclude the following,

(1) The CFD tools can provide precise and reliable results as verified by the ITTC 1957 correlation line comparison. The results show that the CFD method can be employed for estimation of the total resistance of the AUV, even though the shape of the vehicle is complex.

(2) Auto mesh generation with boundary layer inclusion can be used for faster convergence. The convergence time can be significantly reduced by monitoring the object function and controlling the iteration times.

(3) The Design of Experiment optimization design method, one of several optimization tools available in Ansys, was employed for finding the optimal values of three design parameters that would produce a design with the minimum drag force.

(4) The sensitivity of the drag force to each of the design variables was analysed, and as a consequence, it was determined that the angle of attack of the nozzle has the most profound impact on the drag of the vehicle.

ACKNOWLEDGEMENTS

The authors would like thank to Professor Yoshiki Nishi of Yokohama National University for his advice regarding the CFD modelling techniques.

The financial support of this research from the Australian Government's Flagship Collaboration Fund through the CSIRO Wealth from Oceans Flagship Cluster on Subsea Pipelines, and the Australian Research Council is acknowledged and appreciated.

REFERENCES

ANSYS Inc, 2009. *ANSYS CFX-Solver Theory Guide: Release 12.0*. ANSYS Ltd. pp. 46-87.

Barros, E. A., 2006. Progress towards a method for predicting AUV derivatives, *IFAC Conference on Maneuvering and Control of Marine Craft*.

Barringhaus, D. and Olds, R., 2007. *How a Marine Nozzle Works*. http://www.propellerpages.com.

Edward, V. Lewis., 1988. *Principles of Naval Architecture*: Second Revision, Volume 2. The Society of Naval Architects and Marine Engineers, pp. 7-15.

Hoerner, S.F., 1965. *Fluid-Dynamic Drag, Hoerner Fluid Dynamics*. Brick Town, N.J.

Myring, D. F., 1976. A Theoretical Study of Body Drag in Subcritical Axisymmetric Flow. *Aeronautical Quarterly*, 27(3), pp.186–94, 14, 15, 43.

Michael, V. Jakuba., 2003. *Modeling and Control of an Autonomous Underwater Vehicle with Combined Foil/Thruster Actuators*, Massachusetts Institute of Technology, pp.33-62.

Nishi, Y., Kashiwagi, M., Koterayama, W., Nakamura, M., Samuel, S.Z.H., Yamamoto, I. and Hyakudome, T., 2007. Resistance and Propulsion Performance of an Underwater Vehicle Estimated by a CFD Method and Experiment, *ISOPE '07*, Lisbon, Spain.

Phillips, A., Furlong, M. and Turnock, S.R., 2007. The Use of Computational Fluid Dynamics to Access the Hull Resistance of Concept Autonomous Underwater Vehicles, *OCEAN '07 IEEE Aberdeen*.

Wilcox, D.C., 1998. *Turbulence Modeling for CFD*, DCW Industries.